Effects of microbial spatial distribution on organic biodegradation and immobilization of trace metals in co-contaminated soils

Shakil A. Masum, Hywel R. Thomas,*

Geoenvironmental Research Centre, School of Engineering, Cardiff University, CF24 3AA, UK

*Corresponding Author: masumsa1@cf.ac.uk

ABSTRACT

Predicting the transport and fate of organic and inorganic contaminants in co-contaminated soils is challenging, since various complex, inter-related processes are involved. In the presence of soil microbes that metabolise organic compounds (*e.g.*, phenol), the chemical and the physical properties of the soil may alter and consequently affect the transport of inorganic trace metals *e.g.*, Cu, Cd, Ni, Pb. However, the impact of their spatial distributions on the co-transport processes are still poorly understood and rarely available in literature. Here, we distribute the microbial colonies spatially in uniform and various non-uniform configurations and observe that the transport of weakly-sorbed Cd and Ni is greatly influenced by the distance of the colonies from the contaminant source rather than the size of the colonies. Whereas, for strongly-sorbed Pb and Cu, both the distance and the size are important. The spread of phenol in the model domain was substantially restricted by distributing the colonies more towards the transverse direction than in the longitudinal direction of the groundwater flow. In the context of co-contaminated soil remediation, this study demonstrates that optimum

and efficient spatial distribution patterns can be obtained to restrict the spread of both organic and inorganic contaminants, with subsequent reduced environmental impacts.

Keywords: Biodegradation, phenol, bacteria, trace metals, partitioning, remediation

1. Introduction

Waste and wastewater, disposed or discharged from mine tailings, pesticides, pharmaceuticals, metal, and plastic industries, contaminate the surrounding environment with both inorganic and organic pollutants (Nsanganwimana et al., 2014). Trace metals, *e.g.*, cadmium (Cd), nickel (Ni), chromium (Cr), Copper (Cu), lead (Pb), mercury (Hg), arsenic (As), and organic pollutants, *e.g.*, petrochemicals, chlorinated solvents, pesticides, herbicides (Sandrin and Maier, 2003) can be found in those sites. Environmental impact assessment and remediation of co-contaminated sites of such toxic, persistent pollutants is complex and challenging, since various inter-related processes are involved (Olaniran et al., 2013; Song et al., 2017) and different treatment strategies need to be followed (Sandrin and Maier, 2003). Decontamination of metals is primarily based on physico-chemical, electrical and thermal techniques, whereas metabolic degradation via soil microbes is preferred for organic pollutants. The interactions between the pollutants affect their speciation, solubility as well as bioavailability, which can either inhibit or promote the efficiency of their remediation (Jin et al., 2014). This therefore further complicates the remediation of co-contaminated soils and the processes are not yet fully understood (Ye et al., 2017).

Microorganisms, such as bacteria, can utilize organic aromatic carbons as sole substrates for cell growth and maintenance (Ucun et al., 2010), and can provide a pathway for bioremediation. Numerous studies (Said and Lewis, 1991; Kuo and Genthner, 1996; Knight et al., 1997; Yoon, 1998; Roane et al., 2001; Li and Davis, 2008; Kret et al., 2015) were conducted

to estimate and/ or to enhance biodegradation efficiency of organic pollutants, and exhaustive reviews are available in (Nies, 1999; Sandrin and Maier, 2003; Olaniranet al., 2013). Existing literature, to a large extent, is focused on the consequences of metal toxicity on biodegradation and it is well established that the presence of heavy metals, above threshold concentrations, inhibit a wide range of microbial processes including organic biodegradation. In contrast, information regarding the effects of biodegradation on metal transport processes is lacking, despite its importance in the context of co-contaminated sites. A majority of the reported studies were conducted in controlled laboratory experiments where environmental conditions were strictly controlled (Ye et al., 2017). For example, the pH of a system is often regulated to achieve optimum microbial growth and/or maximum biodegradation. However, studies (Garcia et al., 2000; Ucun et al., 2010; Feitkenhauer and Meyer, 2004) that allowed variation or did not strictly regulate the conditions, reported changes in pH with biodegradation.

Ucun et al. (2010) conducted batch experiments in a bioreactor to assess biodegradation of phenol. Although a phosphate buffer system was included to control/ stabilize the pH, reduction was recorded in each experiment. Similar results were reported by Garcia et al. (2000) and Feitkenhauer and Meyer (2004) who investigated removal of phenol and phenolic compounds from wastewater via microbial degradation. Davis et al. (2007) and Prommer et al. (2007) conducted large-scale column experiments and numerical studies respectively, to investigate the effects of increasing acidity on bio-precipitation of trace metals (Cu, Zn and selenium). Ethanol was injected into metal-spiked groundwater under controlled conditions to reduce sulphates into metal sulphides. Along with the robustness of metal bio-precipitation, they observed increased mobility of metals when pH buffering was reduced or exhausted. This is of importance for *in-situ* or field conditions, where suitable pH buffers may not be present or favourable pH conditions cannot be maintained. For example, soils with low organic matter, cation exchange capacity or clay contents exhibit poor pH buffering. Retention and release of

trace metals in soil, to a large extent, is controlled by the solid-solution partitioning behaviour (Tipping et al., 2003) and soil pH can significantly influence this behaviour (Sauvé et al., 2000; Sheppard, 2011).

Studies that reported increasing toxicity on microbial activities with metal concentration were based on pure monocultures (Sandrin and Maier, 2003). In contrast, those that used a consortium of mixed microbial cultures (Capone et al., 1983; Kuo and Genther, 1996; Kang et al., 2016) reported stimulation of microbial activities at low metal concentrations, which elevated to a maximum level before decreasing with increasing metal concentrations. This is mainly associated with the differential inhibition mechanism and the alleviation of competition for resources in a mixed culture of microorganisms (Sandrin and Maier, 2003). Mixed cultures can also exhibit higher resistance to pH, and increased growth, than monocultures (Kolmert and Johnson, 2001; Kang et al., 2016).

A few studies that predict transport and biodegradation of organic pollutants are available in (MacQuarrie and Sudicky, 1990; Frind et al., 1999; Prommer et al., 2002, 2007), but those focused on the transport of both organic contaminants and trace metals coupled with biodegradation are limited. In general, laboratory studies and predictive models consider a uniform distribution of biomass in the experiments or in the model domain. In reality, microbial biomass exists non-uniformly, controlled by attachment and detachment mechanisms imparted by prevailing favourable or unfavourable environmental conditions, respectively, which can give rise to a stochastic distribution (Watnick and Kolter, 2000). The patterns of their distribution can potentially impact the co-transport behaviour of both pollutants, and are therefore, important for environmental impact assessment as well as remediation of co-contaminated sites. However, such studies are rarely available in the literature.

In this study, we use a predictive model (Masum and Thomas, 2018a, b) to investigate the transport and fate of co-discharged organic and inorganic pollutants in the vicinity of a

contaminant source. We consider four heavy metals, *e.g.*, Cu, Ni, Cd, Pb, and phenol as the organic pollutant. Phenol biodegradation is considered to be driven by a microbial community of mixed bacterial species. In this paper, we focus on the distribution patterns of the microbes. We distribute them non-uniformly, both symmetrically and asymmetrically, as well as uniformly throughout the model domain to envisage the extent of their impacts on the co-transport behaviour of the pollutants. We aim to identify the key factors and features in the distribution patterns that perhaps facilitate the remediation of co-contaminated soils effectively and minimise overall environmental impacts.

2. Methodology

Here we present the theoretical basis of the transient model that includes fluid flow, contaminants flow, microbial growth kinetics and their coupled interactions. We also present the phenol degradation reaction, pH dependent solid-solution partitioning and the adopted coupling procedure.

2.1 Phenol biodegradation

Phenol, phenolic compounds are often found in industrial wastewater which are carcinogenic and imposes sever risk to public health. Due to their persistent, non-degradable nature, USEPA has listed phenols as one of the priority pollutants (Ucun et al., 2010). Phenol is an inhibitory substrate; at higher concentration it slows down microbial growth and consequently the degradation. Both aerobic and anaerobic microorganisms can be used to degrade phenols. Nonetheless, aerobic microbes are more efficient, as they grow rapidly and usually convert organic substrates into inorganic compounds, *e.g.*, CO_2, cell mass and water (Sandrin and Maier, 2003). Here, we consider the following biodegradation reaction (Bethke, 2008) of phenol (C_6H_5OH).

$$C_6H_5OH_{(aq)} + 7O_{2(aq)} + 3H_2O \rightarrow 6HCO_3^- + 6H^+ \quad \text{(R1)}$$

The degradation reaction produces acid that may reduce the pH level of a system in absence of other chemical processes or suitable pH buffers.

2.2 Solid-solution partitioning coefficient (K_d) and pH

The partitioning or distribution coefficient correlates the solid phase metal concentrations to the liquid phase at equilibrium. A large number of K_d values were compiled and categorised with respect to solution pH, organic and total metal concentration (by Sauvé et al. (2000)) or clay content (by Sheppard (2011)). They found the best fit to data using linear regressions and developed empirical relationships to predict K_d as a function of pH, organic matter content, total metal concentration/clay content. Although inclusion of soil organic matter, total metal, clay content improved the regression to some extent, both studies reported that the dominant variable to predict K_d in soil is pH. In their data, Sauvé et al. (2000) included soil studies only and excluded specific clays or oxides and, therefore, we adopt their empirical relationships specific to the metals of interest (Table 1) in this study.

Table 1 Solid-solution partitioning of the four heavy metals considered in this study. Partitioning coefficient, K_d (l/kg) as a function of pH, reported by Sauvé et al. (2000).

Heavy metals	**pH dependent K_d relationships**
Cd	$\log_{10}(K_d) = 0.49pH - 0.60$
Pb	$\log_{10}(K_d) = 0.49pH + 1.37$
Cu	$\log_{10}(K_d) = 0.27pH + 1.49$
Ni	$\log_{10}(K_d) = 0.72pH - 1.75$

2.3 Theoretical description

We denote $c_d(\mathbf{x},t)$ as the concentration of a solute in soil solution at point $\mathbf{x} \in \boldsymbol{\Omega}$, where $\boldsymbol{\Omega}$ represents the soil domain. Solute transport is governed by the liquid phase velocity, hydrodynamic dispersion and retardation at the solid-liquid interface. We express the governing equations as:

$$R_D^i \frac{\partial c_d^i(\mathbf{x},t)}{\partial t} + \mathbf{v_l}(\mathbf{x},t) \cdot \nabla c_d^i(\mathbf{x},t) - \nabla \cdot \left(\boldsymbol{D}_h^i \nabla c_d^i(\mathbf{x},t) \right) = s_d^i \qquad \mathbf{x} \in \boldsymbol{\Omega} \qquad (1)$$

$$\mathbf{v_l}(\mathbf{x},t) = -\frac{k_{sat}}{n\gamma_l} \nabla u_l(\boldsymbol{x},t) \qquad \mathbf{x} \in \boldsymbol{\Omega} \qquad (2)$$

$$R_D^i = 1 + \frac{\rho_b K_d^i}{n}. \qquad (3)$$

Here $R_d$is the retardation factor, $\mathbf{v_l}(\mathbf{x},t)$ is the seepage velocity for horizontal flow, $\boldsymbol{D}_h$ is the matrix of hydrodynamic dispersion coefficients, $s_d$is the sink/source term (excluding sorption). $u_l(\mathbf{x},t)$ is the liquid pressure field, k_{sat} is the saturated hydraulic conductivity and, γ_l is the unit weight of water. n is porosity, $\rho_b$is the soil bulk density and $K_d$is the soil solid-solution partitioning coefficient. Superscript ^{i} represent the i^{th} component in soil solution, *i.e.*, one of the four heavy metals or phenol in this case. The hydrodynamic dispersion coefficient includes both mechanical dispersion and effective diffusion. Please see section S1.0 in the Supporting Information (SI) for details. We consider that the liquid is incompressible and therefore, $\nabla \cdot \mathbf{v_l} = 0$

In nature, soil microbes exist both in sessile and planktonic states. However, sessile communities, or biofilms, are often the dominant state of microorganisms in a range of surface and near surface environments compared to the planktonic phases (Flemming and Wuertz, 2019). We express the sessile microbial community (or biofilm) zones in the soil domain as $\boldsymbol{\Omega^b}$, and $\boldsymbol{\Omega^b} \subset \boldsymbol{\Omega}$. We write the mass conservation equations for microbes in solid and liquid phases as:

$$\frac{\partial}{\partial t} c_b^s(\mathbf{x},t) = (r_+ - r_-) c_b^s(\mathbf{x},t) \qquad \text{[sessile]} \quad \mathbf{x} \in \boldsymbol{\Omega^b} \qquad (4)$$

$$\frac{\partial c_b^l(\mathbf{x},t)}{\partial t} + \mathbf{v_l}(\mathbf{x},t)\cdot\nabla c_b^l(\mathbf{x},t) - \nabla\cdot\left(\boldsymbol{D}_h\nabla c_b^l(\mathbf{x},t)\right) = (r_+ - r_-)c_b^l(\mathbf{x},t)\ \text{[plnk]} \qquad \mathbf{x}\in\boldsymbol{\Omega} \qquad (5)$$

where $c_b^l$is the concentration of planktonic microbes in the soil solution, $c_b^s(\mathbf{x},t)$ is the concentration of attached/sessile microbes per unit volume of the soil at point $\mathbf{x}\in\boldsymbol{\Omega^b}$. Please note that a number of microbial species may exist in the sessile state and here we consider their total amount. r_+ and r_- represent microbial growth and decay rates, respectively. Microbial growth via substrate metabolism is usually explained by the standard Monod Kinetic when it is assumed that the growth is not limited by an oxidiser. The assumption limits the application of the model to scenarios where supply of oxygen is abundant and it does not limit the growth, such as, in Ucun et al. (2010). The standard Monod kinetics do not include substrate inhibition effects. Metabolism of an inhibitory substrate, *e.g.* phenol, can be calculated using the Haldane equation.

$$r_+ = k_+\left(\frac{c_d^p}{K_s'+c_d^s}\right) \qquad \text{[Monod kinetic]} \qquad (6)$$

$$r_+ = k_+\left(\frac{c_d^p}{K_s'+c_d^p+\frac{(c_d^p)^2}{K_i'}}\right) \qquad \text{[Haldane kinetic]} \qquad (7)$$

where k_+ is the specific substrate utilisation rate, c_d^p is the concentration of phenol in soil solution, K_s' is the Monod half-saturaiton constant. K_i' is the inhibition constant which measures the sensitivity to inhibition by an inhibitory compound (Ucun et al., 2010). We calculate the loss or removal of the substrate phenol from soil solution using:

$$s_d^p = {}^{r_+}/_{Y} \qquad (8)$$

where *Y* is the growth yield, *i.e.*, the amount of biomass created per unit phenol degradation. s_d^p represents the sink term of phenol in Eq.(1).

We calculate the pH change associated with phenol degradation from reaction R1. We use the reaction stoichiometry and Eq.(8) to estimate the amount of proton released into the soil solution and feed that into the empirical relationships, listed in Table 1, to obtain the metal

specific K_d values. The transient model solves the (relevant) governing transport equations, reaction and sorption in each time-step to calculate the primary variables: chemical concentration c_d, planktonic cell concentration c_b^l, sessile cell concentration c_b^s, and porewater pressure u_l; and pH, which are then updated for the next time-step. The detailed development of the model including theoretical formulation and numerical framework is available in (Masum and Thomas, 2018a).

3. Results and discussion

3.1 Effects of biodegradation on system pH and solid-solution partitioning coefficient

In this section, firstly, we compare a laboratory phenol biodegradation experiment results (which is obtained from the literature) with the model predicted results. Then we calculate the impacts of phenol degradation on the system pH and, consequently, on the solid-solution partitioning coefficients of the metal contaminants.

Ucun et al. (2010) conducted biodegradation of phenol under isothermal conditions in a batch reactor using activated sludge. The inoculum was a phenol degrading mixed culture grown aerobically from activated sludge with phenol as the sole source of carbon. Experiments were performed at various initial phenol concentrations ranging from 50 to 1000 mg/l. Each batch was prepared with 15-day old sludge and during the tests a sufficient supply of air was maintained (to agitate the contents of the reactor) to ensure that the microbial growth was not limited by oxygen. Data were collected at pre-defined time intervals until the phenol was exhausted in the reactor. To estimate phenol volatilization, air stripping tests were conducted during the experiments; however, no volatilization of phenol was detected.

Here we simulate the following batch-experiment: initial phenol concentration of 250 mg/l, microbial biomass concentration of 420 mg/l and pH at 6.3. In the experiment, biomass was defined as Mixed Liquor Suspended Solids (MLSS) (as inoculum). Here we assume that

the MLSS is mainly consists of microorganisms and therefore equals to the biomass concentration. The simulation parameters (Ucun et al., 2010): k_+=3.31×10^{-5} s^{-1}, Y=0.45, K_s'=11.13 mg/l, K_i'=250.88 mg/l, r_-=1.67×10^{-7} s^{-1}.

The simulation period was 5 h and the results are presented in Fig.1. The model predicted results show good agreement with the experimental results when microbial growth kinetics is described by the Haldane equation. The result of phenol degradation using standard Monod kinetics, which does not account for substrate inhibition, leads to rapid degradation of the organic pollutant as indicated by the experimental results.

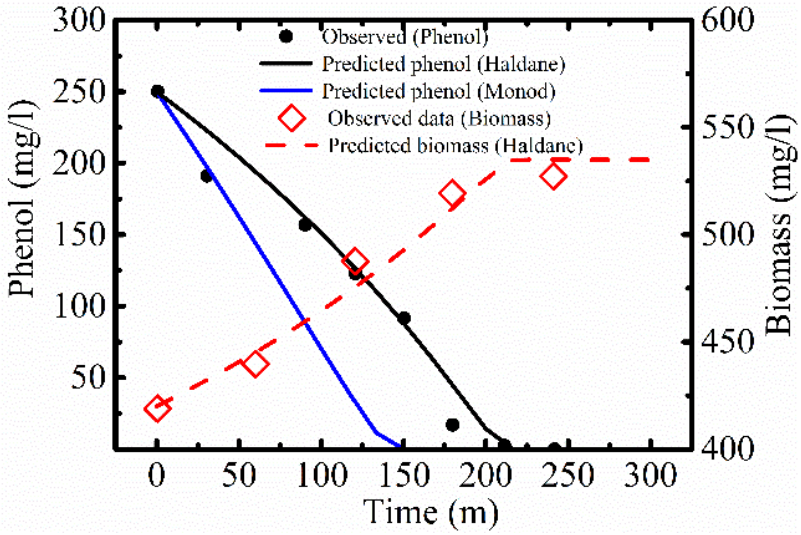

Figure 1. Comparison of experimental data and model predicted results of phenol biodegradation in a batch reactor.

In their experiment, Ucun et al. (2010) used phosphate buffers to ensure favourable pH conditions for the optimal biomass growth and the maximum phenol degradation. The time dependent pH variation data are not available, but they reported that the minimum pH during this experiment dropped to 5.5 from the initial 6.3, despite the presence of the buffer in the solution. Here, we are interested to observe the pH variation when the condition is not regulated

during the simulation, *i.e.*, in absence of a suitable pH buffer. We present the result in Fig.2a, which shows a significant drop of pH from 6.3 to 2.2 based on the reaction, R1. pH decreases sharply at the beginning, by the [H+] released from phenol degradation and slows down as the phenol is depleted. A mixed microbial consortium usually supports a large bio-kinetic pH range and, therefore, sustain optimum growth regardless of the pH variation (Kang et al. 2016; Kolmert and Johnson, 2001).

Finally, we calculate the partitioning coefficients of Cu, Pb, Cd and Ni for the predicted pH range using the corresponding linear regressions in Table 1 and present in Fig.2b. The results show a few orders of magnitude variation in the K_d values for most of the heavy metals. Ni shows the most sensitivity while Cu shows the least. The order of sensitivity follows: Ni > Cd > Pb > Cu.

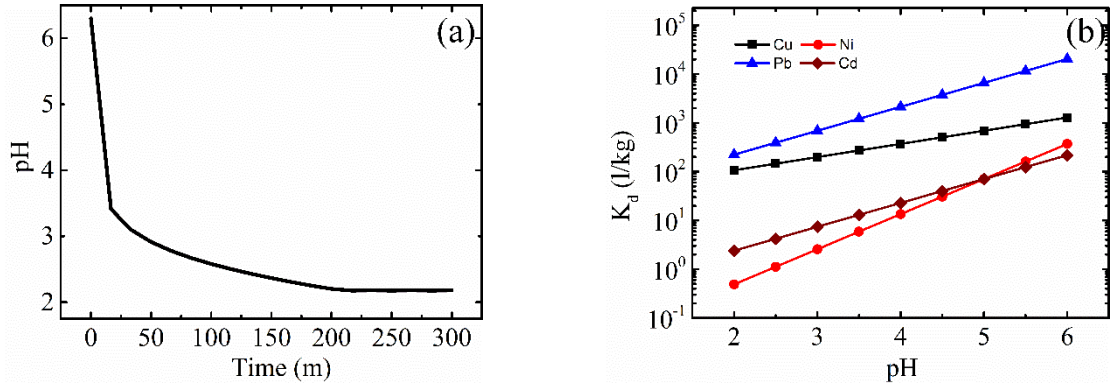

Figure 2. Evolution of (a) pH in the batch solution, and (b) the corresponding solid-solution partitioning coefficient (K_d) following the regression relationships presented in Table 1.

3.2 Co-transport of heavy metals and phenol under simultaneous phenol biodegradation

In the previous section we have demonstrated the effect of phenol degradation on solution pH and estimated metal specific K_d values for that pH variation. Here, we predict the co-transport behaviour of organic phenol and the heavy metals in soil when discharged simultaneously from a contaminant source. Since, microbial colonies in nature usually exist

non-uniformly or stochastically, on a number of scales, we evaluate several distribution patterns. We run a set of simulations by distributing sessile microbial community zones ($\boldsymbol{\Omega^b}$) symmetrically, asymmetrically, as well as uniformly throughout the study area ($\boldsymbol{\Omega}$). The conceptual distribution patterns are presented in Fig.3. We focus on the size of the community zones in terms of number colonies and their distances from the contaminant source in the configurations. We include the uniform distribution scenario, because conventional models often assume this distribution and it aids the comparison with non-uniform distribution scenarios. We assume that the soil is homogenous, the microbial community is an assemblage of species with differential optimum growth rates and favours a large bio-kinetic pH range (*e.g.*, 2.0-8.0) for growth, and metal sorption dominates over any other chemical reaction.

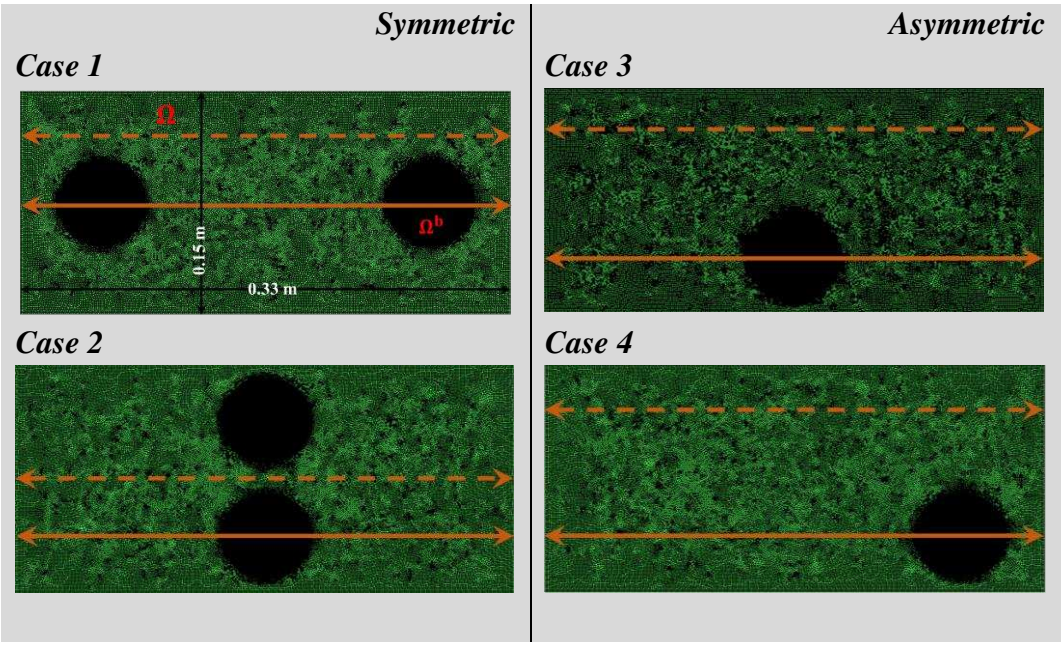

Figure 3. Conceptual illustration of symmetric (Case 1, Case 2) and asymmetric (Case 3, Case 4) distribution in the study domain. The black circular patch represents a community of diverse microbial (bacteria) species. S*olid-lines* and *dashed-lines* mark the locations where the results of metal concentration profiles are taken for Fig.7.

3.2.1 Simulation data

At present, no laboratory or field data, relevant to this study, is available in the literature. The simulations are therefore, strictly, part of a conceptual modelling study to understand the effects of these spatial distributions of microbial communities that can degrade phenol and, perhaps, consequently affect the mobility of the inorganic heavy metals. We have considered a representative study domain and simulated various scenarios. For example, concentrations of heavy metals and organic pollutants at the source can widely vary. We have considered their proportionate concentrations (*e.g.* equal and double) in the simulations, to investigate how do these variations influence co-transport behaviours. Microbial kinetics parameters, such as, substrate utilisation rate, substrate inhibition factor, yield, *etc*. are species dependant and can vary from site to site. In the simulations, we have used the microbial kinetics data of Ucun et al. (2010). Moreover, we have conducted a sensitivity analysis of these parameters and simulated microbial growth kinetics using a number of datasets from the literature on phenol biodegradation, to demonstrate the reliability of the data used in the simulations.

3.2.2 Model domain, initial and boundary conditions

We consider a 0.33 m by 0.15 m model domain consisting of silty soil with negligible clay content. The soil is initially free of any contaminates, *i.e.*, initial concentration of phenol, Cd, Cu, Ni, Pb=0.0 mg/l and pH=6.0. Initial concentration of sessile biomass, c_b^s=0.001 mg/m^3 of soil. In symmetric (Case 1, Case 2) and asymmetric (Case 1, Case 2) scenarios, the initial biomass is contained within the circular community zone (radius=3 cm) presented in Fig.3. Concentration of planktonic microbes in the soil is negligible and therefore, c_b^l=0.0. At the left boundary, *e.g.*, x=0, we consider fixed concentrations of phenol=2.0 mg/l, Cd=1.0 mg/l, Cu=1.0 mg/l, Pb=1.0 mg/l and Ni=1.0 mg/l. Hydraulic head at the left and right boundaries are 12.2 m and 10.2 m, respectively. Simulation runtime is 30 d or 720 h.

Table 2. Parameter values for co-transport simulations

Parameters	Values	Comments
Porosity, n	0.49	
Hydraulic conductivity, k_{sat}	7.2×10^{-6} m/s	(Singh and Gupta, 2000)
Coefficient of longitudinal dispersion, α_L	0.033 m	
Coefficient of transverse dispersion, α_T	0.003 m	
Diffusion coefficient of Cu in water, D_0^{Cu}	1.27×10^{-9} m^2/s	(Lide, 1994)
Diffusion coefficient of Pb in water, D_0^{Pb}	9.45×10^{-10} m^2/s	(Lide, 1994)
Diffusion coefficient of Cd in water, D_0^{Cd}	7.2×10^{-10} m^2/s	(Lide, 1994)
Diffusion coefficient of Ni in water, D_0^{Ni}	1.15×10^{-9} m^2/s	(Lide, 1994)
Solid-solution partitioning of phenol, K_d^{phenol}	2.812 l/kg	(Khan and Anjaneyulu, 2005)
Soil bulk density, ρ_b	1330 kg/m^3	
Specific growth rate, k_+	3.31×10^{-5} s^{-1}	(Ucun et al., 2010)
Yield coefficient, Y	0.45	(Ucun et al., 2010)
Monod half-saturation constant, K_s'	11.13 mg/l	(Ucun et al., 2010)
Inhibition constant, K_i'	250.88 mg/l	(Ucun et al., 2010)
Cell death rate, r_-	3.18×10^{-7} s^{-1}	(Taylor and Jaffe, 1990)

3.2.3 Results

The model parameters are listed in Table 2. We present the results of phenol, pH and biomass evolution in Fig.4 and in Fig.5a-5e, respectively. The non-uniform distribution results are plotted at the centre of each circle for Case 1-4 (Fig.3). Fig.5f shows the biomass concentration profile along the length of the domain for uniform distribution after 30 d or 720 h. We also present the contour plots of phenol and pH, obtained at the end of the simulation, in Fig.6.

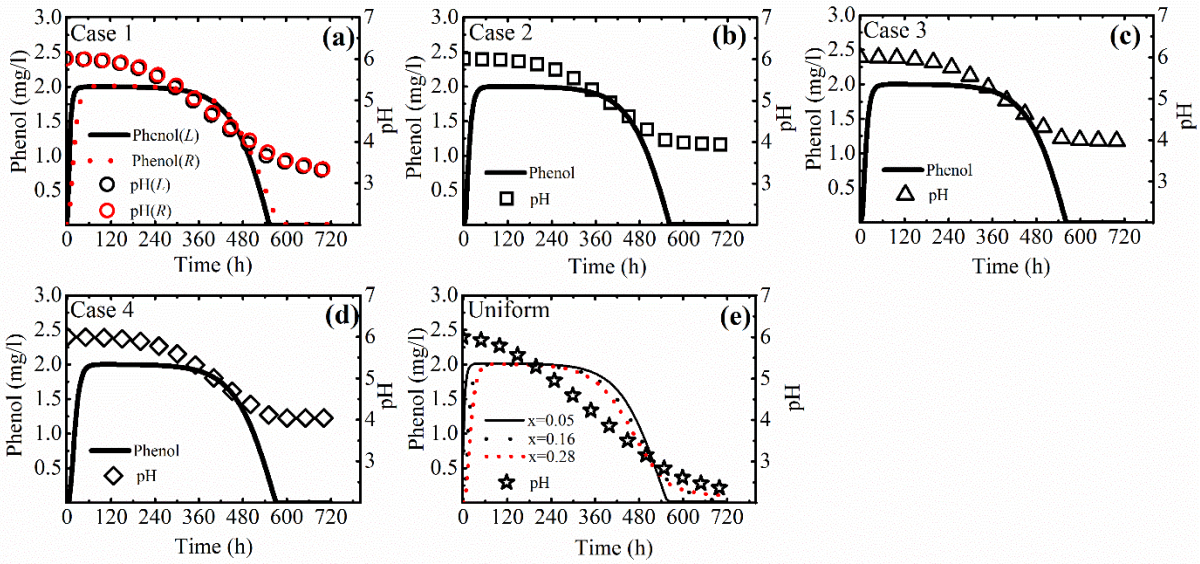

Figure 4. Phenol and pH evolution during the simulation in symmetric (a) Case 1, (b) Case 2; asymmetric (c) Case 3, (d) Case 4; and in (e) uniform distribution scenarios. The results are plotted at the centre of the circles for non-uniform distribution (Fig.3) and at x=0.05, 0.165, 0.28 m for uniform distribution. (L) and (R) in (a) represent the left and right circles of Case 1 distribution, respectively. The *left-vertical-axis* scales phenol and the *right* pH. Please note that the pH evolution for uniform distribution in (e) is presented for x=0.05 m only, since negligible differences were observed in the results at x=0.165 and 0.28 m.

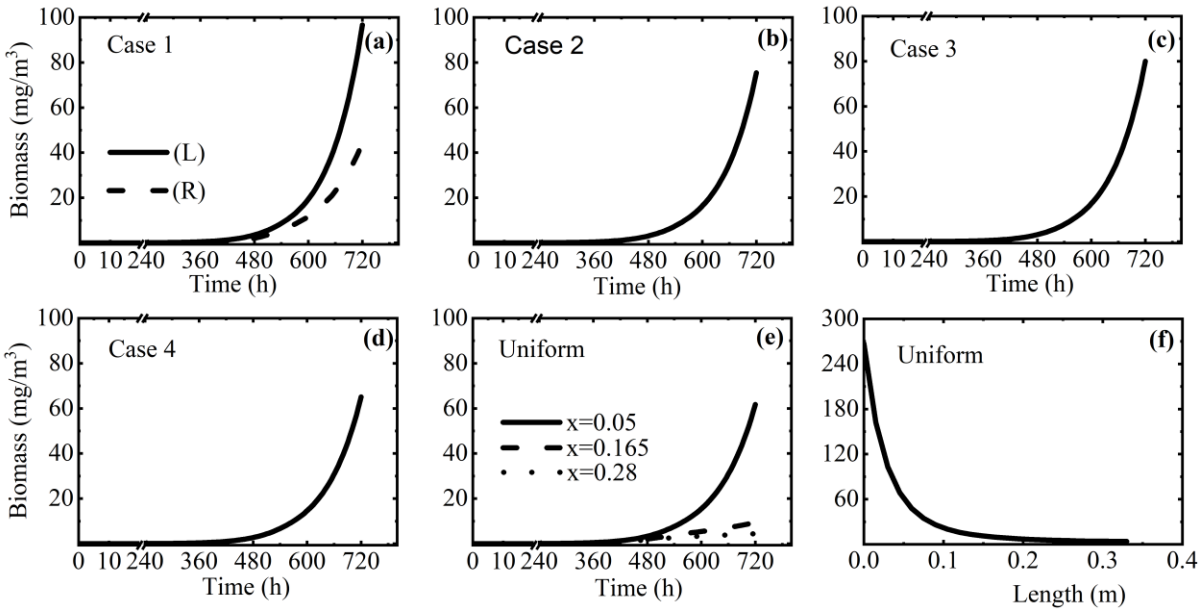

Figure 5. Biomass growth during the simulation in symmetric (a) Case 1, (b) Case 2; asymmetric (c) Case 3, (d) Case 4; and in (e) uniform distribution scenarios. (f) Biomass concentration along the length of the sample at the end of the 720 h simulation period. The results are plotted at the centre of the circles for non-uniform distribution (Fig.3) and at x=0.05, 0.165, 0.28 m for uniform distribution. (L) and (R) in (a) represent the left and right circles of Case 1 distribution, respectively.

In every scenario (Fig.4), phenol concentration increases rapidly to the boundary concentration of 2.0 mg/l, due to the fast advection in the soil. The elevated concentration persists until the microbial community is large enough to make any noticeable change via biodegradation. Fig.5 results show that biomass grows very slowly up until 360 h and, thereafter, exponentially. At this point 40 pore volumes have been moved through the domain. Microbial growth is higher near the source than away from it. This is due to faster supply and recharge of phenol in the vicinity of the source than that of the distant microbes. The maximum biomass growth is observed at the source, 267.2 mg/kg, in case of uniform distribution (Fig.5f). Biomass concentrations for non-uniform distribution patterns, *i.e.*, case 1 (L), case 1(R), case 2, case 3 and case 4 are 96.7, 43.7, 75.4, 79.9, 65.0 mg/kg, respectively (Fig.5a-5e). It is obvious that the symmetric Case 1(R) result in Fig.5a shows higher accumulation of biomass than the result plotted at x=0.28 m for uniform (Fig.5e) scenario, although they represent the same location in the domain. This is because of the intermittent presence of the microbial community (in the former) rather than their continuous presence (in the later). Microbes near the source hinder the supply of phenol to the rest of the domain. Together with Fig.4, Fig.5 results indicate that microbial growth continues to the end of the simulation, despite the phenol being exhausted within the biomass cells between 555-580 h in all cases. The hypothesis is tested in the Fig.A1 of the Appendix. Fig.A1 presents the phenol concentration profiles along the length of the

sample, and the biomass concentrations across the 6 cm biofilm circles, at various simulation periods, for Case 1 distribution. At the early stages (5 d), when the biomass amount is relatively small, phenol concentration across the sample remains high. As the biofilm growth continues, the phenol concentration within the circular patches reduces sharply, although it remains relative higher in the rest of the domain. Despite the continuous biofilm growth, no deviation is observed between the 25- and 30-day phenol concentration profiles indicating that the biofilms are large enough to metabolise the supplied phenols. This is also noticeable in Fig.6a where the phenol is exhausted within the community zones, depleted in the surrounding area and flowing with the soil solution. Fig.4 results show that the solution pH evolves conversely to the biomass. Phenol biodegradation drives the production of protons, as per reaction R1 and reduces the solution pH. The reduction occurs spontaneously, since no buffer or pH-adjustment was considered in the simulations. The largest pH drop, from 6.0 to 2.3, is observed (Fig.6b) in the uniform scenario and then in Case 1(L) (pH=3.2). These are correlated with the higher biomass growth (observed in Fig.5), phenol metabolism and proton release. Although, the biomass concentrations in Fig.5a show significant variations between case 1(L) and (R) results, variation in pH evolution is negligible (Fig.4a). The protons/ [H+] generated in the left circular zone are transported to the right with the flowing water, which elevate the [H+] concentration at that point. Case 2 and 3 show a similar trend and magnitude which complements their corresponding biomass growth. The lowest pH reduction is observed in Case 4 (Fig.4d & 6b), where the distance of the microbial colony from the source is longer than any other cases presented here.

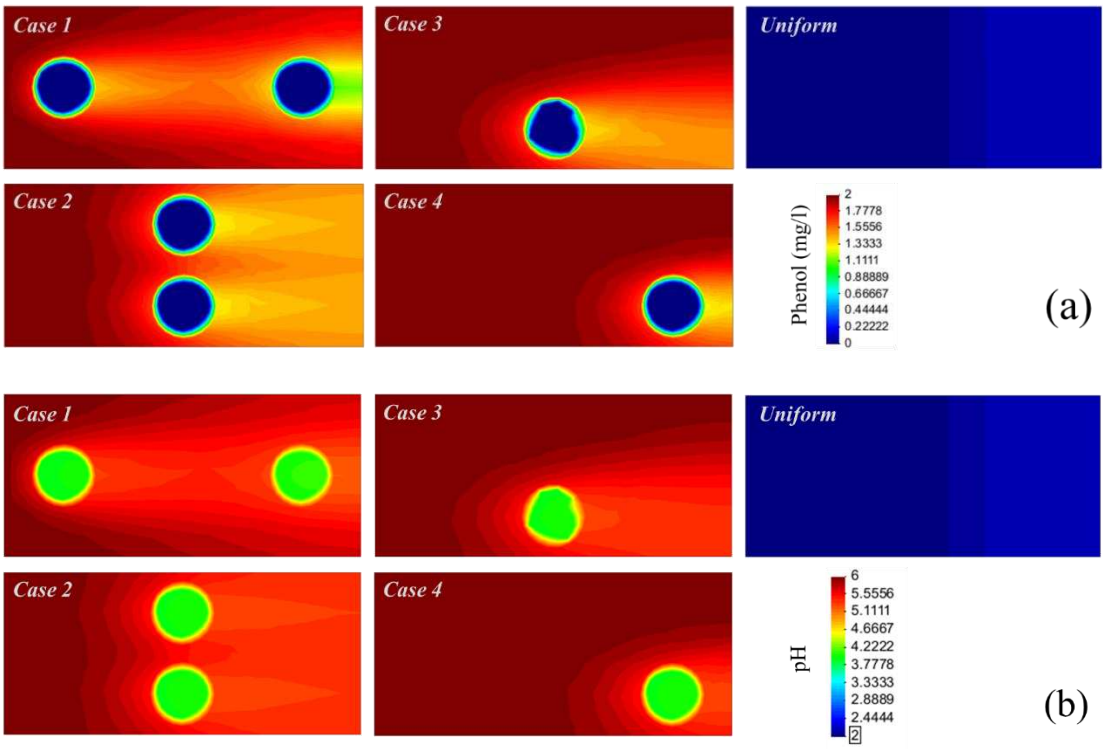

Figure 6. Contour plots of (a) phenol and (b) pH distribution in the model domain at the end of 30 d simulation period

In Fig.7, we present the concentration profiles metal contaminants along the length of the model domain. Cu, Ni, Cd and Pb were co-transported in the soil with the organic phenol. The profiles are plotted at the end of the simulation along the lines presented in Fig.3. The 'fix pH' results represent the scenarios where a suitable phenol-degrading community is not available and, therefore, the system pH remain unchanged (at 6.0 in this case), *i.e.*, constant K_d. The results indicate that metal transport is associated with the aforementioned pH evolution in the study area (Fig.4 and 6b). Metals spread the most with the flowing water when the microbial community is considered to be distributed uniformly throughout the domain. We observed the largest pH drop in this case, suggesting a significant impact on the K_d values. We have seen in the previous subsection that the sensitivity of K_d towards pH varies from metal to metal. Weakly-sorbed or less retarded metals, *e.g.*, Cd and Ni spread similarly in both Case 1 and in uniform distribution scenarios. Transport of these metals are also large in the Case 2 symmetric

distribution. The deviation between concentration profiles (the *solid-* and *dashed-line*s), are negligible in symmetric distribution scenarios, suggesting similar transport behaviour across the domain. To further investigate the importance of the locations of the colonies, we have presented additional distribution scenarios in Fig.S3 of the SI, namely Case S1 and S2. Configuration of the colonies in Case S1 are similar to the Case 2 but located at a longer distance from the source (centre of the $\boldsymbol{\Omega^b}$'s is at x=0.28). Ni transport reduces significantly in this case, 0.53 and 0.16 mg/l at x=0.15 and 0.30, respectively (Fig.S3e). Therefore, an increase of 11.5 cm in distance results into 44.8% to 80% reduction of Ni transport with respect to Case 2. The asymmetric distributions (Case 3 and 4) show lower mobility and less spread of the metal contaminants. Although the area of microbial colony in Case 3 is half of that of the Case 2, metals transport similarly, near the source, in these cases. For example, at x=0.15, Cd=0.98 and 0.95 mg/l, Ni=0.96 and 0.91 mg/l for Case 2 and Case 3, respectively. However, away from the source large deviation is observed. At x=0.30 these values are Cd=0.82 and 0.72 mg/l, Ni=0.80 and 0.56 mg/l. Transport of these metals are slowest in Case 4 distribution (at x=0.15, Cd=0.80 mg/l and Ni=0.50 mg/l). Unlike the symmetric distribution cases, where these metals transport similarly in the study domain, the asymmetric distributions show clear variations. The deviation between the *solid-* and *dashed-line*s are noticeable in the Fig.7 results for Cd and Ni. We also present the contour plots of Ni as an example in Fig.S1 (of SI), which displays highly skewed contours near the microbial community zone in asymmetric distributions (Case 3 and Case 4). However, this lessens away from the community zone suggesting differential transport behaviour in the model domain. In these simulations, the microbial community zones ($\boldsymbol{\Omega^b}$) occupy 11.4% and 5.7% of the total domain for symmetric (Case 1 & 2) and asymmetric (Case 3 & 4) distributions, respectively. The area of the microbial zone in Case S2, presented in Fig.S3, is same as the Case 3 or Case 4, but located closer to the source (the centre of $\boldsymbol{\Omega^b}$ is at x=0.05 which is same as the Case 1L circle presented in Fig.3). Ni transport (Fig.S3e) in this

case is same as the uniform and the Case 1 distribution scenarios (Fig.7), which suggests that the distance of the colonies from the source has more influence on over the size of the overall colonies. Therefore, a microbial colony that occupy only 5.7% of the total area can yield same transport and spread of the weakly-sorbed metals as the uniform distributions, depending on their locations in the soil sample/ study area.

The strongly-sorbed metals, *e.g.*, Pb and Cu show marginal or unnoticeable variations between asymmetric distribution cases and their concentration profiles are either analogous (Case 4) or close (Case 3) to the 'fix pH' results (Fig.7). We observe the largest spread in the uniform distribution scenario (Pb=0.5 mg/l at x=0.061) and then in Case 1 (Pb=0.5 mg/l at x=0.028) where the colony is located at a close proximity to the source. For Cu, these values are 0.16 and 0.10 m. Although the microbial colonies occupy 11.4% of the total domain and located closer to the source in Case 1 scenario, transport of Pb and Cu is significantly less than the uniform distribution. Therefore, both the location and the size of the colonies are important for the transport of strongly-sorbed metals.

Further the distance and smaller the size, their impact diminishes, and the metal transport is mediated by the advective-dispersive transport (as if) with a constant retardation throughout the space. The concentration profiles of these metals do not show any deviation between the *solid-* and *dashed-line*s (Fig.7) for either symmetric or asymmetric distributions which are either due to strong retardation in soil or their less sensitivity to pH variation or both.

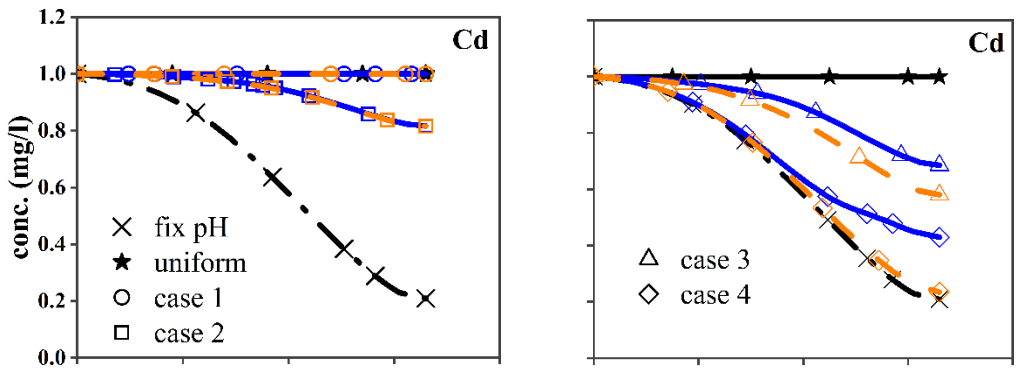

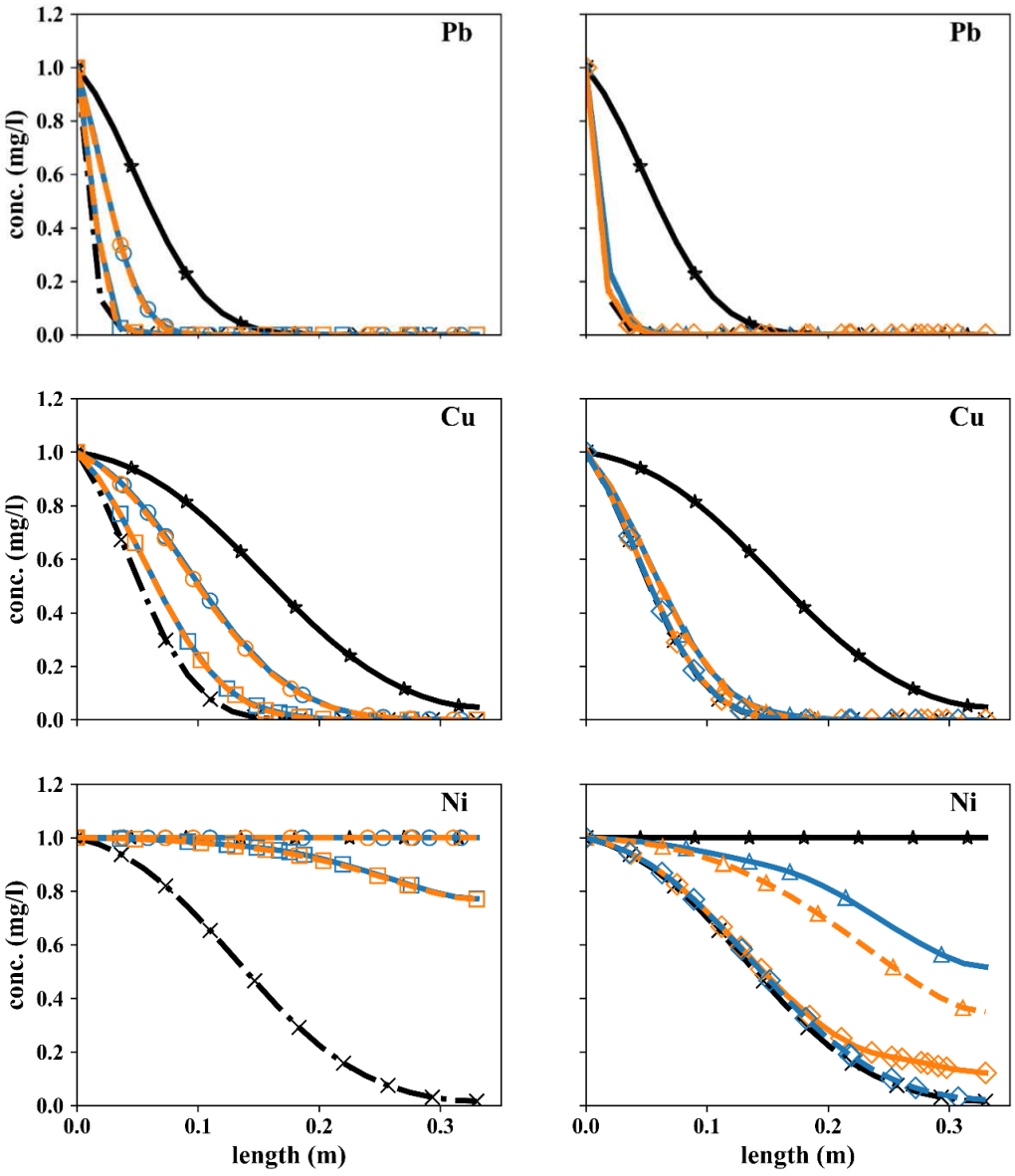

Figure 7. Concentration profiles of Cd, Pb, Cu and Ni along the length of the sample at the end of the 30 d simulation period. The symbols represent (○) Case 1, (□) Case 2, (Δ) Case 3, (◇) case 4, and (☆) uniform distribution scenarios, presented in both plots. *Solid-lines* and *dashed-lines* represent concentration profiles through the centre of the circles and away from the circles (Fig.3), respectively. The symbol (×) represents 'fix pH' simulation scenario where pH change is ignored, *i.e.*, constant-K_d.

Therefore, no differential transport is observed in the model domain. We have presented the contour plots of Cu in Fig.S2 (SI) which shows inconspicuous distortion of the contours.

We observe that the phenol degradation in the entire domain occurs when the microbes are distributed uniformly across the domain (From Fig.6a). However, this also results into accelerated transport and maximum spread of the inorganic contaminants. In context of co-contaminated site remediation, non-uniform spatial distributions provide few alternatives. When the colonies are located in the transverse direction of the groundwater flow, *e.g.* Case 2 and S1, substantial reduction of phenol occurs is the wider area, especially beyond the colonies, and depending on their distances from the source significant immobilisation of metal can also be achieved. If the colonies are located along the groundwater flow direction (Case 1), the phenol depletion occurs in specific areas. Therefore, an appropriate configuration can be chosen to achieve significant removal of organic contaminant while minimising the co-transport of inorganic contaminants.

The results in Fig.4-7 are based on a large hydraulic gradient or seepage velocity that amplifies the effect of microbial spatial distribution on the transport of co-contaminants. High advection facilitates quick and adequate supply of the growth substrate to the microbial colonies. However, in field conditions, the hydraulic gradients can be much lower. Simulation results for such a situation are presented in Fig.A1 and A2 of the Appendix. The simulation conditions and parameters are same as those presented in Section 3.2.2, except the hydraulic head boundaries. In this simulations, the hydraulic head gradients at the left and the right boundaries are 10.213m and 10.2m, respectively, which results into a gradient of 0.04 across the sample domain. In comparison to Fig. 6a, the results in Fig.A2 shows significantly small spread of phenol ever after 30 days of simulation for all patchy distribution cases. Phenol depletion and consequent biofilm growth is only visible in the Case 1 scenario where the microbial colony is closer to the source. In all other cases, sufficient supply of phenol substrate is yet to reach to the microbes. The effect of reduced phenol transport and microbial growth on the spread of Cd is presented in Fig.A3. The pH of the sample domain remains unaffected in

Case 2-4 scenarios. Although the pH in Case 1 distribution shows noticeable reduction, due to the low advective flow, the spread of Cd remains insignificant and follows the predicted profiles of the other distribution cases. This also highlights the effect/ contribution of water flow rate on the overall co-transport behaviours (microbially influenced) of the contaminants.

So far, we have simulated the scenarios where phenol concentration at the source is twice the concentration of heavy metals at the source. We also investigated the scenarios for an equal proportion of organic and inorganic contaminants at the boundary, *i.e.*, at x=0 we considered fixed concentrations of phenol, Cd, Cu, Pb and Ni=1.0 mg/l; while the other conditions, parameters and simulation runtime remained unchanged. We present the results of Ni in Fig.8 for 30 d simulation period and compare them with the results presented in Fig.7. The *unfilled-symbols* represent the results of 2.0 mg/l phenol at the boundary (*i.e.* previous simulation), while the *filled-symbols* represent the 1.0 mg/l results (*i.e.,* current simulation). Fig.8a shows the comparison of biomass growth between the two different boundary conditions for Case 1(L) distribution..

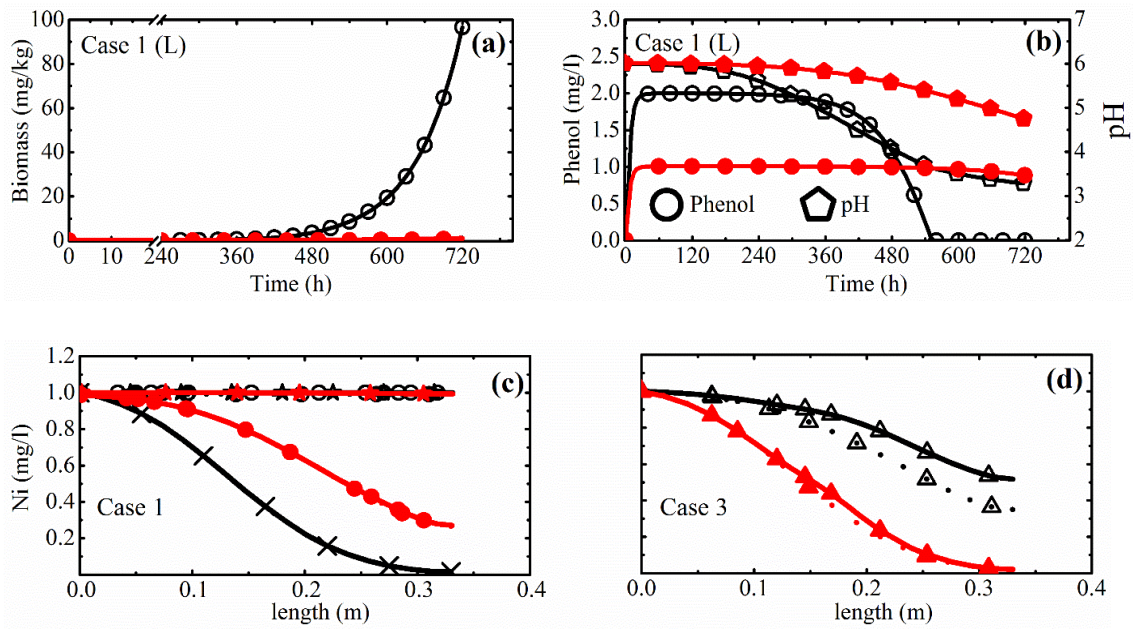

Figure 8: Impacts of phenol and heavy metal proportions at the source concentration on the co-transport behaviour. Evolution of (a) biomass, (b) phenol and pH for the Case 1(L) symmetric distribution scenario. In (b), the symbol (○) scales phenols to the *left-vertical* axis and (⬠) pH to the *right-vertical*

axis. Ni concentration profiles along the samples for (c) Case 1(L) symmetric distribution and (d) Case 3 asymmetric distribution scenarios. The *filled-symbols* represent the 1.0 mg/l simulations while the *unfilled-symbols* represent 2.0 mg/l phenol at the source boundary. The remaining definition of the graphs in (c) and (d) are same as in Fig.7. Simulation period 30 d.

We observe that when phenol concentration is halved at the source, biomass growth reduces significantly, 0.78 mg/kg, during the same period of time. Phenol depletion and pH reduction are significantly small in comparison to the previous simulation (Fig.8b). We present the concentration profiles of Ni in Fig.8c and Fig.8d for Case 1 and Case 3 distributions, respectively, as well as compare them with the results presented in Fig.7. Ni spreads similarly in both set of simulations for uniform distribution; however, it retards significantly for Case 1 and Case 3 scenarios. For example, at 0.2 m distance from the source a 30% reduction of Ni concentration is observed, in Case 1, when the phenol concentration is halved. In Case 3, the observed reduction is 50% approx. Microbial growth slows down with the reduction of substrate concentration and consequently the impacts of biodegradation on the heavy metal transport. Likewise the previous set of simulations, the extents of metal spread in this set of simulation is larger in Case 1 than in Case 3 which show that the location of the bacterial colony and their size remain substantial. However, if the simulation period is extended the growth as well as the impacts becomes more apparent. Please see the results presented in Fig.S4 of the SI for a 45 d (1080 h) simulation period

The results and analysis presented in this section suggest that both the locations of microbial communities and their distribution patterns influence the co-transport processes. Laboratory experiments that aim to measure such transport behaviour in soils, usually consider spiking the samples with bacterial culture to generate a pseudo uniform distribution. But soil heterogeneities might prevent their uniform presence throughout the laboratory samples, and /or, more obviously, in the field conditions. The findings of this study provide useful insight to the extents to which this uncertainty matters, i.e., the discrepancies between the batch test data and the field/ calibrated model data.

3.2.4 Limitations, uncertainty, and sensitivity of the model data/ parameters

Growing biofilms occupy the pore spaces in a porous medium and alleviate the available flow channels. This can eventually affect the hydraulic conductivity of the medium. In this study, the impacts of biofilm growth on the saturated hydraulic conductivity has been neglected which perhaps resulted into an overestimation of advective transport of the contaminants. The limitation will be addressed in future investigations.

For field scale applications, reliable data on site-specific K_d values are essential, since the precision of model predicted metal transport results depends on the accuracy of the correlative/ regression relationships, presented in Table 1. Sites, where soil is partially saturated (rather than fully saturated), reduced fluid flow may hinder supply and recharge of organic substrates and affect microbial growth as well as contaminant transport. Quantity of organic and inorganic pollutants at the source may often vary from site to site. We demonstrated that the higher the concentration of organic compound, the faster the microbial growth and the larger the spread of metal contaminants, and *vice-versa*. This is expected in soils with weak pH buffer where microbial degradation of organic compounds can alter the pH. Soils that are strong in buffering pH are expected to be less sensitive to pH change due to microbial processes and in such cases reactive transport of heavy metals can be predicted with a fixed solid-solution partitioning approach, given that sorption is dominant over other chemical reactions.

We have mentioned previously that the microbial kinetics data is species dependent. To demonstrate the reliability of the data used in the simulations we compared them with existing data in the literature on phenol degradation and presented the results in Table S1 and Fig.S5 of the Supporting Information. The results show that the parameter data and the microbial growth kinetics lies well within the range available for several bacterial cultures. Biomass growth and pH evolution (associated with phenol degradation) occurs rapidly when the values of substrate utilisation rate are higher and/ or the half-saturation constants are lower. We also conducted a

sensitivity analysis of the microbial growth parameters and observed their impact on the spread of heavy metals (*e.g.* Ni). The results are presented in Fig.S6 of the Supporting Information. The results show that substrate utilisation rate is the most sensitive parameter and then the half-saturation constant, therefore, they should be estimated with great care. The inhibition constant and the yield are found to be least sensitive. We observed that the Ni spread reduces significantly for an order of magnitude reduction in substrate utilisation rates (from $\mathcal{O}(10^{-1})$ to $\mathcal{O}(10^{-2})$) and/ or half-saturation constants (from $\mathcal{O}(10^{1})$ to $\mathcal{O}(10^{0})$).

From the aforementioned discussion, we suggest that the site-specific information and accuracy of data will eventually improve the quantitative aspect of the presented results. However, the qualitative aspects and analyses of microbial spatial distribution impacts on the transport behaviour of co-contaminants, observed (and reported) in this study, will remain unchanged.

4.0 Conclusions

In this study, we observed that the co-transport behaviour of organic and inorganic pollutants is influenced by the spatial distribution of microbes capable of degrading the organic pollutant. Biodegradation of phenol affected the retardation and consequently the transport of Cd, Pb, Cu and Ni by altering their solid-solution partitioning, which was considered to be a function of soil pH. Partitioning of Cd and Ni showed more sensitivity to pH variation than Cu and Pb based on the linear-regression relationships considered in this paper. Due to its low retardation, phenol transported faster than the metal contaminants in the soil and the elevated concentration level persisted until the growth of soil microbes was significant.

Biodegradation depleted phenol in the entire study area when the microbes were distributed uniformly throughout the domain. However, this also resulted in the largest spread of the metal contaminants. When non-uniform distributions were considered, the spread of

weakly-sorbed metals (Cd, Ni) was primarily influenced by the distance between the microbial colonies and the contaminant source, and then by the size of the area occupied by these colonies in the study domain. Even a microbial colony that occupies a small percentage of the total area, can accelerate the spread of these metals as large as the uniform distribution given that the colony is located at a close proximity to the source. Further away from the source, their impact on the transport reduces. However, the spread of strongly-sorbed, slow moving metals (Cu, Pb) depended on both the distance and the size of these colonies.

Phenol spread in the model domain was substantially restricted by distributing the colonies more towards the transverse direction than the longitudinal direction of the groundwater flow. When located along the longitudinal direction, phenol spread was larger and depleted at specific locations of the domain.

We also observed that the proportion of organic contaminant at the source could influence the co-transport behaviours of inorganic contaminants by either retarding or accelerating the relevant processes. However, the impacts of microbial spatial distributions on the transport remain evident. In the context of co-contaminated soil remediation, this study demonstrates that optimum and efficient distribution patterns can be obtained to restrict the spread of both organic and inorganic contaminants or to remediate them. Therefore, risk assessments or remediation strategies should consider the locations of native microbial pools or the spatial distributions of applied external/ engineered microbes. However, to upscale or to apply the results of this study in the field, given the associated complexities, including heterogeneity, biomass effect on hydraulic conductivity, mobile and sessile biomass interaction, dispersion etc. is challenging.

Appendix

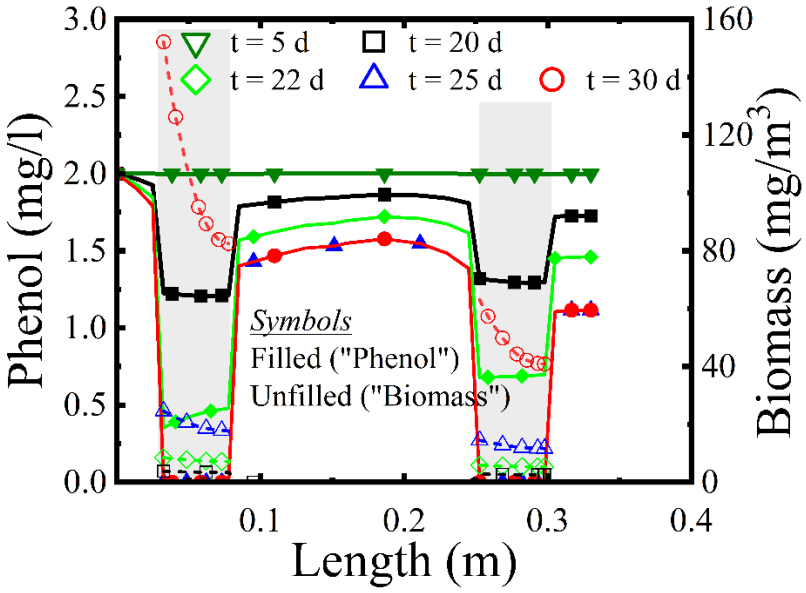

Figure A1: Phenol and biomass concentration profiles along the length of the sample after 5, 20, 22, 25 and 30 days for Case 1 distribution scenario. The shaded areas represent the locations of the circular microbial colonies in the model domain.

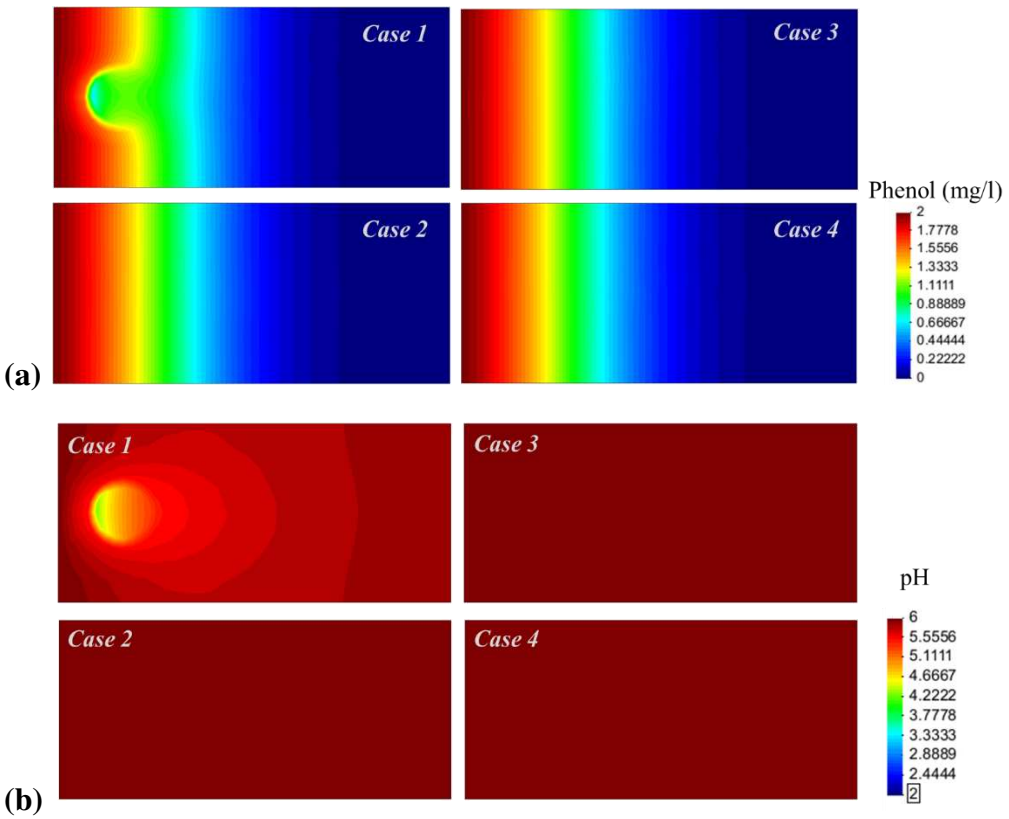

Figure A2: Contour plots of (a) phenol and (b) pH distribution in the model domain at the end of 30 d simulation period. The initial and boundary conditions, and model parameters are same as in the Section 3.2.2 except the hydraulic head values at the boundaries. The hydraulic heads at the left and right boundary are respectively 10.213m and 10.2 m, which is equivalent to a hydraulic gradient of 0.04 across the sample.

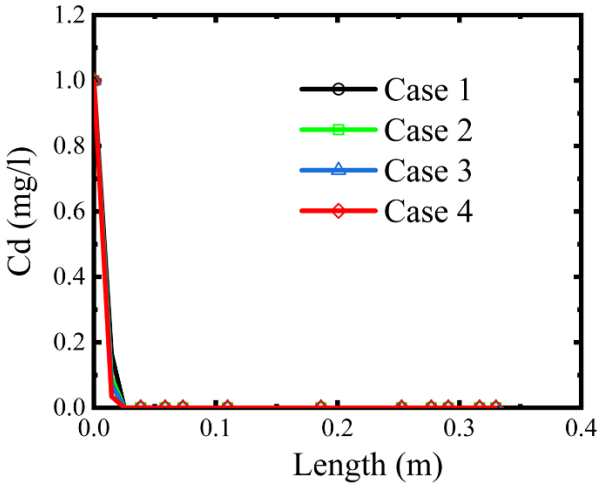

Figure A3. Concentration profiles of Cd along the length of the sample at the end of the 30 d simulation period for various distribution scenarios. The plots refer to the simulations conducted for a hydraulic gradient of 0.04 across the sample.

Acknowledgment

Shakil A. Masum is funded by the Welsh European Funding Office through the Flexible Integrated System (FLEXIS) project. This financial support is gratefully acknowledged.

Reference cited

Angle JS, Chaney RL. 1989. Cadmium resistance screening in nitrilotriacetate-buffered minimal media. *Appl. Environ. Microbiol.* 55:2101–2104.

Bethke CM. 2008. Geochemical and Biogeochemical Reaction Modelling, 2nd Edition, Cambridge University Press: New York, NY.

Capone DG, Reese DD, Kiene RP. 1983. Effects of metals on methanogenesis, sulfate reduction, carbon dioxide evolution, and microbial biomass in anoxic salt marsh sediments. *Appl. Environ. Microbiol.* 45:1586–1591.

Davis AC, Patterson BM, Grassi ME, Robertson BS, Prommer H, Mckinley AJ. 2007. Effects of increasing acidity on metal(loid) bioprecipitation in groundwater: column studies. *Environ. Sci. Technol.* 41:7131-7137.

Feitkenhauer H, Meyer U. 2004. Software sensors based on titrimetric techniques for the monitoring and control of aerobic and anaerobic bioreactors. *Biochem. Eng. J.* 17:147–151.

Flemming HC, Wuertz S. 2019. Bacteria and archaea on earth and their abundance in biofilms. *Nat. Rev. Microbiol.* 17(4):247-260.

Frind EO, Molson JM, Schirmer M. 1999. Dissolution and mass transfer of multiple organics under field conditions: the Borden emplaced source. *Water Resour. Res.* 35:683-694.

Garcia IG, Pena PRJ, Venceslada JLB, Martin AM, Santos MAM, Gomez ER. 2000. Removal of phenol compounds from olive mill wastewater using Phanerochaete chrysosporium, Aspergillus niger, Aspergillus terreus and Geotrichum candidum. *Process Biochem.* 35:751–758.

Jin J, Sun K, Wu F, Gao B, Wang Z, Kang M, Bai Y, Zhao Y, Liu X, Xing B. 2014. Single-solute and bi-solute sorption of phenanthrene and dibutyl phthalate by plant- and manure-derived biochars. *Sci Total Environ.* 473–474:308–316.

Kang C-H, Kwon Y-J, So J-S. 2016. Bioremediation of heavy metals by using bacterial mixtures. *Ecol. Eng.* 89:64-69.

Khan Z. Anjaneyulu Y. 2005. Analysis of the distribution coefficients and mobility characteristics of phenols in different soil types. *Environ. Geol.* 48:1-5.

Knight BP, Mcgrath SP, Chaudri AM. 1997. Biomass carbon measurements and substrate utilization patterns of microbial populations from soils amended with cadmium, copper, or zinc. *Appl. Environ. Microbiol.* 63:39–43.

Kolmert A, Johnson DB. 2001. Remediation of acidic waste waters using immobilised, acidophilic sulfate-reducing bacteria. *J. Chem. Technol. Biotechnol.* 76(8):836-843.

Kret E, Kiecak A, Malina G, Nijenhuis I, Postawa A. 2015. Identification of TCE and PCE sorption and biodegradation parameters in a sandy aquifer for fate and transport modelling: batch and column studies. *Environ. Sci. Pollut. Res.* 22:9877-9888.

Kuo CW, Genthner BRS. 1996. Effect of added heavy metal ions on biotransformation and biodegradation of 2-chlorophenol and 3-chlorobenzoate in anaerobic bacterial consortia. *Appl. Environ. Microbiol.* 62:2317–2323.

Li H, Davis AP. 2008. Heavy metal capture and accumulation in bioretention media. *Environ. Sci. Technol.* 42:5247-5253.

Lide DR. 1994. Kehiaian H.V. CRC Handbook of Thermophysical and Thermochemical Data. 1st Edition, CRC Press: Boca Raton, FL.

Nsanganwimana F, Pourrut B, Mench M, Douay F. 2014. Suitability of *miscanthus* species for managing inorganic and organic contaminated land and restoring ecosystem services. A review. *J. Environ. Manage* 143:123-134.

MacQuarrie KTB, Sudicky EA. 1990. Simulation of biodegradable organic contaminants in groundwater 2. Plume behaviour in uniform and random flow fields. *Water Resour. Res.* 26(2):223-239.

Masum SA, Thomas HR. 2018a. Modelling coupled microbial processes in the subsurface: Model development, verification, evaluation and application. *Adv. Water Resour.* 116:1-173

Masum SA, Thomas HR. 2018b. Modelling the effects of pH on subsurface microbial growth processes. *In* Lau TC, Kelso RM (ed), Proceedings of the 21st Australasian Fluid Mechanics Conference. Australasian Fluid Mechanics Society (AFMS), Adelaide, Australia. ISBN 978-0-646-59784-3.

Nies DH. 1999. Microbial heavy-metal resistance. *Appl. Microbiol. Biotechnol.* 51:730-750.

Olaniran AO, Balgobind A, Pillay B. 2013. Bioavailability of heavy metals in soil: Impact on microbial biodegradation of organic compounds and possible improvement strategies. *Int. J. Mol. Sci.* 14:10197-10228.

Prommer H, Barry DA, Davis GB. 2002. Modelling of physical and reactive processes during biodegradation of a hydrocarbon plume under transient groundwater flow conditions. *J. Contam. Hydrol.* 59(1-2):113-131.

Prommer H, Grassi ME, Davis AC, Patterson BM. 2007. Modelling of microbial dynamics and geochemical changes in a metal bioprecipitation experiment. *Environ. Sci. Technol.* 41:8433-8438.

Roane TM, Josephson KL, Pepper IL. 2001. Microbial cadmium detoxification allows remediation of co-contaminated soil. *Appl. Environ. Microbiol.* 67:3208–3215.

Said WA, Lewis DL. 1991. Quantitative assessment of the effects of metals on microbial degradation of organic chemicals. *Appl. Environ. Microbiol.* 57:1498–1503.

Sauvé S, Hendershot W, Allen H. 2000. Solid-solution partitioning of metals in contaminated soils: dependence on pH, total metal burden, and organic matter. *Environ. Sci. Technol.* 34(7):1125-1131

Sandrin TR, Maier RM. 2003. Impact of metals on the biodegradation of organic pollutants. *Environ. Health Perspec* 111(8):1093-1101.

Sheppard SC. 2011. Robust prediction of Kd from soil properties for environmental assessment. *Hum. Ecol. Risk Assess.* 17:263-279.

Singh DN, Gupta AK. 2000. Modelling hydraulic conductivity in a small centrifuge. *Can. Geotech. J.* 37(5):1150-1155.

Song B, Zeng G, Gong J, Liang J, Xu P, Liu Z, Zhang Y, Zhang C, Cheng M, Liu Y, Ye S, Yi H, Ren X. 2017. Evaluation methods for assessing effectiveness of in situ remediation of soil and sediment contaminated with organic pollutants and heavy metals. *Environ. Int.* 105:43-55.

Taylor SW, Jaffe PR. 1990. Substrate and biomass transport in porous medium. *Water Resour. Res*. 26(9): 2161-2169.

Tipping E, Rieuwerts J, Pan G, Ashmore MR, Lofts S, Hill MTR, Farago ME, Thornton I. 2003. The solid-solution partitioning of heavy metals (Cu, Zn, Cd, Pb) in upland soils of England and Wales. *Environ. Pollut.* 125:213-225.

Ucun H, Yildiz E, Nuhoglu A. 2010. Phenol biodegradation in a batch jet loop bioreactor (JLB): kinetics study and pH variation. *Bioresour. Technol.* 101:2965-2971.

Watnick P, Kolter R. 2000. Biofilm, city of microbes. *J. Bacteriol.* 182(10):2675-2679.

Ye S, Zeng G, Wu H, Zhang C, Dai J, Liang J, Yu J, Ren X, Yi H, Cheng M, Zhang C. 2017. Biological technologies for the remediation of co-contaminated soil. Crit. Rev. Biotechnol. 37(8):1062-1076.

Yoon KP. 1998. Isolation and characterization of Pseudomonas sp. KM10, a cadmium and mercury-resistant and phenol-degrading bacterium. J. Microbiol. Biotechnol. 8:388-398.